Consistent large-scale response of hourly extreme precipitation to temperature variation

Haider Ali[1], Hayley J. Fowler[1], Geert Lenderink[2], Elizabeth Lewis[1], David Pritchard[1]

1. School of Engineering, Newcastle University, Newcastle upon Tyne, UK

2. Royal Netherlands Meteorological Institute, De Bilt, the Netherlands

Abstract

Hourly precipitation extremes can intensify with temperature at higher rates than expected from thermodynamic increases explained by the Clausius-Clapeyron (CC) relationship (~6.5%/K), but local scaling with surface air temperature is highly variable. Here we use daily dewpoint temperature, a direct proxy of absolute humidity, to estimate at-gauge local scaling across six macro-regions for a global dataset of over 7000 hourly precipitation gauges. We find scaling rates from CC to 2xCC at more than 60% of gauges, peaking in the tropics at a median rate of ~1.5CC. Moreover, regional scaling rates show surprisingly universal behaviour at around CC, with higher scaling in Europe. Importantly for impacts, hourly scaling is persistently higher than scaling for daily extreme precipitation. Our results indicate greater consistency in global scaling than previous work, usually at or above CC, with positive scaling in the (sub)tropics. This demonstrates the relevance of dewpoint temperature scaling to understanding future changes.

1 Introduction

Short-duration precipitation extremes can cause flash floods, landslides, and debris flows with little or no warning, leading to serious socioeconomic impacts (Fadhel et al., 2018). Hence, they are highly relevant in the design of water resource and stormwater drainage infrastructure systems, especially in urban areas due to their strong surface impermeability (Ali & Mishra, 2017). Insight into the impacts of warming on sub-daily (particularly hourly to 3-hourly) extreme precipitation may, therefore, be crucial for societal decision-making for climate adaptation (Bader et al., 2018). Studying changes to historical precipitation extremes can aid the understanding of potential future changes to extreme precipitation (Allen & Ingram, 2002). Previous studies have reported that climate warming and urbanisation are intensifying observed daily precipitation extremes globally (Alexander, 2016; Ali et al., 2018; R. Barbero et al., 2017; Westra et al., 2014) with some evidence suggesting enhanced increases in observed extreme hourly precipitation intensities (Guerreiro et al., 2018; Li et al., 2020).

The intensification of precipitation extremes with warming can be explained thermodynamically from the increase in humidity, or water vapour, of the atmosphere. The Clausius-Clapeyron (CC) relationship has therefore been used as a benchmark to interpret change to extreme precipitation (Fischer & Knutti, 2016; O'Gorman, 2015). This relation links air temperature and atmospheric humidity when the air is saturated, giving an increase in humidity of 6-7% per degree warming (Trenberth et al., 2003). Under the assumption of constant relative humidity, which is partly supported by climate modelling results and physical reasoning at least over (relatively) wet surfaces, the actual humidity of the air increases at the same rate.

Recent studies have confirmed an approximately CC rate of increase in long-term trends in observations and projections of daily extreme rainfall (Fischer & Knutti, 2016; Guerreiro et al., 2018; Rajczak & Schär, 2017; Scherrer et al., 2016) when averaged globally or over large regions and mostly using large-scale temperature rise or even global temperature rise. To investigate the relationship between warming and the intensification of rainfall extremes, however, a common approach uses scaling between surface air temperature (SAT) and precipitation extremes. This approach, here called "apparent" scaling following the terminology introduced by Bao et al. (2017),

employs short-term variations in temperature and precipitation, mostly caused by day-to-day synoptic variability up to seasonal variations, to derive dependencies of precipitation extremes on temperature.

Results of studies using apparent scaling have shown a wide range of behaviour. Often, behaviour close to the CC rate is obtained (Ali et al., 2018; Gao et al., 2018; Wasko et al., 2016). However, for some regions signs of super-CC behaviour, exceeding the CC rate, have been found for sub-daily (mostly hourly) precipitation (Peter Berg et al., 2013; Lenderink et al., 2011; Lenderink & Van Meijgaard, 2010; Park & Min, 2017). On the other hand, negative scaling rates, signifying decreases in precipitation intensity with warming have been found for subtropical and tropical regions (Hardwick Jones et al., 2010; Vittal et al., 2016). Where scaling rates with SAT deviate significantly from CC (Ali et al., 2018; Hardwick Jones et al., 2010; Zhang et al., 2017) this has been shown to be a result of confounding factors such as local cooling effects (Ali & Mishra, 2017; Bao et al., 2017), moisture limitations at higher temperatures (Barbero et al., 2018; Gao et al., 2018; Lenderink et al., 2018; Trenberth & Shea, 2005), temperature seasonality (Ali et al., 2018; Zhang et al., 2017), statistical methods and inappropriate modelling assumptions (Pumo et al., 2019; Wasko et al., 2015) and mixing of different rainfall types (Berg & Haerter, 2013; Molnar et al., 2015). Moreover, the localised effects of large-scale circulation patterns enhanced local moisture availability through upward motions and moisture convergence, and local-scale dynamics can influence scaling rates (Ali & Mishra, 2018; Guerreiro et al., 2018; G. Lenderink et al., 2017; Pfahl et al., 2017).

This diversity of behaviour, and the complexity of the physical processes involved, has led to a large debate in the literature on the potential use of apparent scaling, and how it could be related to climate change. Here, we show that a considerable part of this controversy can be resolved when using dew point temperature (DPT), which measures the actual humidity of the air instead of the humidity at saturation, extending several recent studies (Ali & Mishra, 2017; Barbero et al., 2017, 2018; Gao et al., 2018; Geert Lenderink & Attema, 2015). Ali et al. (2018) showed consistent global scaling of daily extreme precipitation at the CC rate using DPT as a scaling variable instead of SAT. While we fully acknowledge the complexity issues described above, we also note that there is some evidence of surprising similarities in scaling dependencies between different areas and links between longer-term variations in DPT and hourly precipitation extremes (Lenderink et al., 2011; Lenderink & Attema, 2015).

Therefore, in this paper, we focus on the following questions. Are negative scaling rates, in particular for subtropical and tropical areas, an artefact of the use of SAT in most scaling studies? Do we find more universal behaviour across the globe using DPT, and how much could this behaviour deviate from CC rates? How widespread is super-CC behaviour in hourly extremes, and do scaling rates of hourly extremes exceed those of daily extremes?

Here we use gauge observations of hourly precipitation (PPT) from the Global Sub-Daily Rainfall (GSDR) dataset (Lewis et al., 2019) and daily DPT from HadISD (Dunn et al., 2012, 2016) to establish, for the first time, the scaling relationship between extreme hourly precipitation and daily DPT at a global scale. We examine six main regions: the USA, Australia, Europe, Japan, India and Malaysia with a total of 7088 gauges which have at least 12 years of data (Barbero et al., 2019a) (start and end year varies between 1979-2014). We estimate scaling rates across these selected regions at different spatial scales. For every gauge, we estimate the scaling using the classic binning method (Lenderink & Van Meijgaard, 2008) (BM) and check the consistency of our results against other scaling methods (quantile regression, QR; Ali et al., 2018) and removing the seasonality in DPT (Zhang et al., 2017) (ZM)). The Methods section provides details on the datasets, their quality control, and the methods used to estimate scaling relationships at these different spatial scales.

2 Data and Methods:

PPT and DPT data

We obtained hourly precipitation data (PPT) from the Global Sub-Daily Rainfall (GSDR) dataset (Lewis et al., 2019) which was compiled under the Global Water and Energy Exchanges (GEWEX) Hydroclimatology Panel INTENSE project (Blenkinsop et al., 2018) and has been used in many recent studies (Barbero et al., 2017, 2019a, 2019b; Guerreiro et al., 2018; Li et al., 2020; Moron et al., 2019). The GSDR data has been quality-controlled using 25 different checks to identify and remove a range of errors, such as physical and spatial consistency issues, spikes and flat lines (streaks) (Blenkinsop et al., 2017; Lewis et al., 2018). We selected six macro-regions where data was available: The United States of America (US), Australia, Europe, Japan, India and Malaysia to provide a comprehensive global study covering different climate zones with large latitudinal and elevation ranges. The gauges in the USA were of mixed-precision (0.25 mm and 2.54mm), therefore, all the gauges in the USA were explicitly processed to have a consistent 2.54 mm precision (Barbero et al., 2019b). Although the spatial and temporal coverage of the GSDR dataset is not uniform, we ensured a sufficient length of precipitation data for estimating scaling. Therefore, we only considered PPT stations which have at least 12 years of data with less than 20% missing hours in any given year (start and end year varying between 1979-2014; Fig. S4).

We obtained daily dewpoint temperature data (DPT) from the Met Office Hadley Centre observations dataset: HadISD (version 2.0.2.2017f) (Dunn et al., 2019, Lewis et al., 2019). This is a global dataset (8103 stations) spanning 1/1/1931 to 12/12/2017 and is based on the Integrated Surface Dataset (ISD) from the National Oceanic and Atmospheric Administration's (NOAA's) National Climatic Data Center (NCDC).

The details on quality-control of DPT data, pairing DPT with PPT data, and pooling PPT-DPT pairs is mentioned in Supplemental Information.

Methods:

We used three methods for estimating scaling: (a) Binning Method, (b) Quantile regression, and (c) Zhang et al. (2017) method (ZM).

To apply the BM, we first considered all wet hours (with precipitation ≥ 0.1mm, except for the US and Japan for which the minimum amount was 2.5mm and 1mm respectively) for each station's PPT-DPT pair. We then placed data into 12 bins of equal size, sorted from the lowest to highest DPT, and estimated the 95^{th}/99^{th} percentile of PPT (P95/P99) and the mean DPT for each temperature bin. We excluded the first and last bins from the scaling estimate to avoid any noise or absurd DPT values which may be outliers to climatology resulting from very specific circulations. We fitted a linear regression on the logarithm of P95 and mean DPT for the second bin to the second last bin (2to2last) and from the second bin to the bin where the maximum of P95 occurred (2toBP), which is given by:

$$\log(P95) = \alpha + \beta T \quad (1)$$

Then scaling (dP95(%)/K) was then estimated using an exponential transformation of the regression coefficient (β) given by:

$$dP95(\%)/K = 100.(e^{\beta} - 1) \quad (2)$$

QR is similar to BM except there is no assumption of the number and size of bins. The scaling was estimated using equations 1 and 2 for all wet hours for paired PPT-DPT data for a given percentile (99^{th} percentile in our study).

To ensure that the increase in extreme precipitation with DPT is not dominated by seasonal trends in DPT, we also removed the seasonality from the DPT data to estimate the scaling (Ali et al., 2018; Zhang et al., 2017). In the ZM method, we first identify the four months which receive the highest PPT in a year for each location and then estimate the DPT anomalies for these four months. For the

same four months, we normalised the maximum hourly PPT amount by the median of the maximum hourly PPT (for the whole time series for these top four months). We then fitted a Generalized Extreme Value distribution (GEV) to these normalised maximum hourly PPT data using the corresponding DPT anomalies as a covariate on the location parameter in the GEV model (as in Ali et al., 2018).

Moreover, we also examined the latitudinal variation in scaling, and the difference in scaling between dry and wet regions (defined in Donat et al., 2016) and constructed scaling curves for larger regions by pooling all locations within similar climate zones, based on the Koppen-Geiger classification system. We distributed the available 7088 gauges into 5-degree width latitudinal bands (Fig 3a) and estimated the median scaling for each band. Moreover, we grouped the available gauges into dry and wet regions following the classification of Donat et al. (2016). They (Donat et al., 2016) calculated precipitation indices (annual maximum precipitation, Rx1day; and total precipitation, PRCTOT) for each grid cell and normalised them by dividing by the average of the base period (1951-1980). The grid cells with the 30 per cent lowest normalised precipitation index values were labelled as dry and the 30 per cent highest values were labelled wet, respectively. We also constructed scaling curves for the selected regions by pooling all stations with an elevation greater than and less than 400m within a Climate Zone. The choice of the 400m threshold is somewhat arbitrary but is motivated to avoid the mixing of DPT from different altitudes (Lenderink et al. (submitted)). High altitudes have lower DPT than lower altitudes and the mixing of DPT may produce a statistical artefact to artificially flatten the scaling curves. The absolute number of stations pooled within each climate zone is mentioned at the top of each upper panel in Fig 4. All the wet hour PPT-DPT pairs were placed in 2℃ wide bins, ranging from 0℃ up to 28 ℃. From this binned data we then computed the 95^{th}, 99^{th} and 99.9^{th} percentile of the distribution of the wet events (as Lenderink et al., 2017).

3 Results

3.1 Extreme precipitation scaling at station-level and pooled regions

We first examine the scaling rates at individual gauges. We find that the relationship between hourly precipitation and dewpoint temperature is generally consistent with CC (6.5%/K) scaling at most locations across the selected regions. Although spatial variability in scaling is high across regions, a small majority of 60% of gauges show scaling at greater than the CC rate (Fig. 1). The highest regional median scaling rates are observed for Malaysia (11.8%/K) and Australia (8.5%/K). More noteworthy is that around 10% (22%) of locations in Australia (Malaysia) show greater than 2×CC scaling. Using other methods to estimate scaling rates gives consistent results (Fig. S1 and S2). The scaling rates are slightly higher for the warm season (Jun-Aug, except for Dec-Feb for Australia) (Fig. S3).

We now move on to assess whether the record length for an individual hourly precipitation gauge may lead to any bias in scaling rate, by pooling P-DPT pairs for three neighbouring gauges within 30 km distance with elevation difference no greater than 50m (Fig. S4). Note that there is a chance that the same DPT station observations are paired to two or more precipitation gauges. Notwithstanding this limitation, we observe that the pooled median scaling rates are still higher than CC for all regions (Fig. S5), although slightly lower than those for individual gauges (Fig. 1). These show consistently strong relationships between hourly precipitation extremes and dewpoint temperature.

Accumulating the hourly precipitation data to daily totals produces scaling rates consistent with those of Ali et al. (2018) (Fig. 2 and S6), at approximately CC or lower. The results for daily totals from different methods are consistent except for in tropical regions (Malaysia and India). Tropical regions show relatively low-temperature variability, e.g., all hourly precipitation extremes in Malaysia occur in a DPT range of just 20-26 ℃ (Fig. S8). Since BW and QR methods can be affected by seasonality,

in particular, if the DPT range is small, ZM provides a better method to estimate scaling in the tropics (Ali et al., 2018) and this produces consistently higher scaling rates in the tropics (Fig. 2).

We now examine the latitudinal distribution of scaling from hourly precipitation using 5-degree width latitudinal bands, except for 10-20 degrees North (with only 3% of total 7088 gauges), with the distribution of gauges in each latitudinal band shown in Fig 3a. We find that the median scaling is mostly at (or slightly above) the CC rate for all latitudes (Fig. 3b), and that scaling peaks in the Tropics at over 1.5CC. We also examine the difference in overall scaling between wet and dry regions, as classified by Donat et al. (2016). It is important to note that their classification is based only on precipitation (extreme precipitation: annual maximum precipitation, Rx1day; or total precipitation, PRCTOT) and does not account for differences in temperature, humidity, etc. Based on the Rx1day extreme precipitation index and using the 30% highest/lowest gauges to define wet (extreme; blue)/dry (less extreme; red)(Donat et al., 2016), the scaling for the less extreme region (median 9.11%/K) is greater than for the more extreme region (median 7.9%/K). However, classifying based on total precipitation (PRCTOT), we find the scaling is higher for the wet region. The differences between the classification based on the two indices are mainly due to gauges in Europe (which show generally higher scaling rates) falling into different regions in each case. The results are the same when a higher threshold (40%) is used for the classification into wet and dry regions (Fig. S7).

3.2 Scaling curves

We now examine the scaling relation for different climate zones by constructing scaling curves for selected regions. Scaling curves can help visualise the scaling relationship within the full DPT range, unlike scaling rates (Fig. 1 and 2) which are the single values of linear slope (coefficient) across the DPT range. We first split the data into locations higher and lower than 400m altitude (to avoid effects of differences in DPT with altitude), and then pool PPT-DPT pairs within the same climate zone, based on the Koppen-Geiger classification system (Kottek et al., 2006) (Table S2). We use the same methodology as previously to construct scaling curves for each regional climate zone (Fig. 4, upper panels) and compare these to the distribution of scaling rates at individual gauges from Fig. 1 (Fig. 4, lower panels). For the Temperate climate zone C (common to five from six regions where hourly precipitation gauge data is available), scaling curves follow at least the CC rate in all regions (Fig. 4). To summarise, scaling curves for hourly precipitation over large climate regions tend to the CC rate or above, although scaling curves are flatter for gauges at greater height (>400m) compared to lower altitude gauges (<400m). Strikingly, we find that scaling curves for Europe follow 2×CC beyond 12°C (Fig. 4c) which supports the findings of Lenderink and Meijgaard (2008) for the Netherlands. What is also remarkable is that scaling curves are almost universal for the different regions; that is, for a given DPT the values of the different percentiles are very close. The scaling rates derived from these pooled data are also similar, at close to the CC rate or slightly above, with exceptions for the lowest and highest dew point temperatures. However, there are some systematic differences, such as the relatively low intensities in the low DPT range (<10 °C) in Europe.

Examining the distribution of scaling rates estimated at gauge-level, most stations exceed the CC rate, and a small fraction of stations even exceed 2×CC in all four regions for the C climate zone (Fig. 4b, d, f and h). The at-gauge scaling distribution within the C climate zone is similar for locations higher and lower than 400m MSL for Australia and Japan (Fig. 4d, f). On the contrary, there is a significant ($p<0.05$) difference in the at-gauge scaling for Europe, where lower altitude gauges (<400m MSL) show much higher scaling than gauges above 400m MSL (Fig. 4d). In tropical Malaysia (A climate zone), with a very low range in DPT (~21-26°C), scaling curves follow at least the CC rate (Fig. S8). Scaling curves for the US (C and D climate zones) also follow the CC rate beyond 12°C (Fig. S9). Since the measurement precision for rain gauges in the USA is much coarser (2.54 mm) we did not include these results in the main figures.

4 Conclusions and discussion

In this study, we have used observed hourly precipitation and daily DPT to estimate scaling over six macro-regions. At gauge level, we found that scaling rates ranged between CC and 2×CC for more than 60% of gauges. We note that comparatively lower scaling rates at US gauges may be due to their coarse measurement resolution. To remove spatial variability in at-gauge estimates of scaling, from short record lengths and local modes of variability, we assessed various pooling methods. Pooling data for three neighbouring gauges produced reduced scaling rates but with a scaling range between CC and 2×CC for more than 50% of gauges. Moreover, the median scaling is greater than CC for gauges in wet and dry regions. When we further pooled gauges across selected regions within the same Koppen-Geiger climate zone, we found that regional scaling curves consistently follow the CC rate. The exception to this is for Europe where regional scaling for climate zone C is significantly higher than the CC rate for temperatures above 12°C, consistent with findings for the Netherlands (Lenderink & Van Meijgaard, 2008). Our results suggest that by pooling data the influence of local dynamics producing super-CC behaviour is averaged out, resulting in lower scaling rates from the pooled data analyses than from the individual gauges. These local dynamics produce higher super-CC sensitivities in most of the gauges analysed globally. For instance, excess latent heat released during intense short-duration rainfall may enhance scaling (Haerter & Berg, 2009); other mechanisms include intensifying upward within-cloud motions (Lenderink et al., 2017), and increases in moisture-convergence producing larger storms (Pfahl et al., 2017); but see Fowler et al. (submitted) for a comprehensive review. Our results highlight the importance of understanding the thermodynamic and dynamic processes governing precipitation extremes at different spatial scales when estimating future changes.

In summary, we have shown that the scaling of hourly extreme precipitation consistently follows at least the CC rate at a regional scale, and often a super-CC rate at the gauge-level, across regions where hourly data is available. This is a much stronger scaling than that for daily extreme precipitation and adds critical information to the debate on how precipitation extremes may change in the warming climate, particularly pertinent for impacts. Of interest is whether we expect changes to be regionally or locally constrained or enhanced, and why regions like Europe show super-CC scaling rates. It is an open question whether these observed scaling rates are indicative of rates of future change with warming but some evidence from high-resolution convection-permitting modelling now suggests that they may be (Lenderink et al. submitted). Of course, scaling rates may further increase (or decrease) due to other dynamical processes, including changes to large-scale circulation patterns (Pfahl et al., 2017), cloud size and the spatial extent of rainfall events (Lochbihler et al., 2017), storm type (Molnar et al., 2015), and changes to long-term moisture transport patterns (Pfahl et al., 2017). We emphasize that these factors have not been considered explicitly in our scaling approach and further studies are still needed both to understand the processes governing precipitation extremes at different temporal and spatial scales and the potential future changes to these processes. Meanwhile, the observed strong and the surprisingly universal relationship between hourly precipitation extremes and dewpoint temperature has implications for the design of stormwater infrastructure systems, and perhaps provides a way of updating such estimates.

Acknowledgements

This work was supported by the INTENSE project. INTENSE is supported by the European Research Council (grant ERC-2013-CoG-617329). Hayley Fowler is funded by the Wolfson Foundation and the Royal Society as a Royal Society Wolfson Research Merit Award holder (grant WM140025). We thank Markus Donat (University of New South Wales) for providing us with the shapefiles of wet and dry regions. The GSDR dataset will shortly be hosted by the Global Precipitation Climatology Centre at Deutsche Wetterdienst and available through the Copernicus Climate Change Service Climate Data Store. Until then, the data can be obtained from the authors. For raw data sources, see table A1 of

281 doi.org/10.1175/JCLI-D-18-0143.1. HadISD dewpoint temperature data is freely available at
282 https://www.metoffice.gov.uk/hadobs/hadisd/.

283 **Author contributions**

284 HA and GL carried out the analysis. HJF and HA contributed to the design of the methodology. EL
285 and DP produced the quality-controlled hourly precipitation data. All authors discussed the results and
286 contributed to writing the paper.

287 **Competing financial interests**

288 The authors declare no competing financial interests.

289

290 **References:**

291 Alexander, L. V. (2016). Global observed long-term changes in temperature and precipitation
292 extremes: A review of progress and limitations in IPCC assessments and beyond. *Weather*
293 *and Climate Extremes*, *11*, 4–16.

294 Ali, H., Fowler, H. J., & Mishra, V. (2018). Global observational evidence of strong linkage between
295 dew point temperature and precipitation extremes. *Geophysical Research Letters*, *45*(22), 12–
296 320.

297 Ali, H., & Mishra, V. (2017). Contrasting response of rainfall extremes to increase in surface air and
298 dewpoint temperatures at urban locations in India. *Scientific Reports*, *7*(1), 1–15.

299 Ali, H., & Mishra, V. (2018). Contributions of dynamic and thermodynamic scaling in subdaily
300 precipitation extremes in India. *Geophysical Research Letters*, *45*(5), 2352–2361.

301 Allen, M. R., & Ingram, W. J. (2002). Constraints on future changes in climate and the hydrologic
302 cycle. *Nature*, *419*(6903), 228–232.

303 Bader, D. A., Blake, R., Grimm, A., Hamdi, R., Kim, Y., Horton, R., & Rosenzweig, C. (2018).
304 *Urban climate science. In Climate Change and Cities: Second Assessment Report of the*
305 *Urban Climate Change Research Network (ARC3. 2)*. Cambridge University Press.

306 Bao, J., Sherwood, S. C., Alexander, L. V., & Evans, J. P. (2017). Future increases in extreme
307 precipitation exceed observed scaling rates. *Nature Climate Change*, *7*(2), 128–132.

308 Barbero, R., Abatzoglou, J. T., & Fowler, H. J. (2019b). Contribution of large-scale midlatitude
309 disturbances to hourly precipitation extremes in the United States. *Climate Dynamics*, *52*(1-
310 2), 197-208.

311 Barbero, R., Fowler, H. J., Lenderink, G., & Blenkinsop, S. (2017). Is the intensification of
312 precipitation extremes with global warming better detected at hourly than daily resolutions?
313 *Geophysical Research Letters*, *44*(2), 974–983.
314 Barbero, R., Westra, S., Lenderink, G., & Fowler, H. J. (2018). Temperature-extreme precipitation
315 scaling: A two-way causality? *International Journal of Climatology*, *38*, e1274–e1279.
316 Barbero, Renaud, Fowler, H. J., Blenkinsop, S., Westra, S., Moron, V., Lewis, E., Chan, S.,
317 Lenderink, G., Kendon, E., & Guerreiro, S. (2019a). A synthesis of hourly and daily
318 precipitation extremes in different climatic regions. *Weather and Climate Extremes*, *26*,
319 100219.
320 Berg, P., & Haerter, J. O. (2013). Unexpected increase in precipitation intensity with temperature—A
321 result of mixing of precipitation types? *Atmospheric Research*, *119*, 56–61.
322 Berg, Peter, Moseley, C., & Haerter, J. O. (2013). Strong increase in convective precipitation in
323 response to higher temperatures. *Nature Geoscience*, *6*(3), 181–185.
324 Blenkinsop, S., Fowler, H. J., Barbero, R., Chan, S. C., Guerreiro, S. B., Kendon, E., ... & Alexander,
325 L. (2018). The INTENSE project: using observations and models to understand the past,
326 present and future of sub-daily rainfall extremes. *Advances in Science and Research*, *15*, 117-
327 126.
328 Blenkinsop, S., Lewis, E., Chan, S. C., & Fowler, H. J. (2017). Quality-control of an hourly rainfall
329 dataset and climatology of extremes for the UK. *International Journal of Climatology*, *37*(2),
330 722-740.
331 Donat, M. G., Lowry, A. L., Alexander, L. V., O'Gorman, P. A., & Maher, N. (2016). More extreme
332 precipitation in the world's dry and wet regions. *Nature Climate Change*, *6*(5), 508–513.
333 Dunn, R. J. H. (2019). HadISD version 3: Monthly updates. *Met Office Hadley Centre Technical*
334 *Note*.
335 Dunn, R. J., Willett, K. M., Parker, D. E., & Mitchell, L. (2016). Expanding HadISD: Quality-
336 controlled, sub-daily station data from 1931. *Geoscientific Instrumentation, Methods and*
337 *Data Systems*, *5*(2), 473.

Dunn, R. J., Willett, K. M., Thorne, P. W., Woolley, E. V., Durre, I., Dai, A., Parker, D. E., & Vose, R. E. (2012). HadISD: A quality-controlled global synoptic report database for selected variables at long-term stations from 1973–2011. *ArXiv Preprint ArXiv:1210.7191*.

Fadhel, S., Rico-Ramirez, M. A., & Han, D. (2018). Sensitivity of peak flow to the change of rainfall temporal pattern due to warmer climate. *Journal of Hydrology*, *560*, 546–559.

Fischer, E. M., & Knutti, R. (2016). Observed heavy precipitation increase confirms theory and early models. *Nature Climate Change*, *6*(11), 986–991.

Fowler, H.J. *et al*. Intensification of short-duration rainfall extremes with global warming and implications for flood hazard. Submitted to Nature Reviews Earth and Environment, in revision.

Gao, X., Zhu, Q., Yang, Z., Liu, J., Wang, H., Shao, W., & Huang, G. (2018). Temperature dependence of hourly, daily, and event-based precipitation extremes over China. *Scientific Reports*, *8*(1), 1–10.

Guerreiro, S. B., Fowler, H. J., Barbero, R., Westra, S., Lenderink, G., Blenkinsop, S., Lewis, E., & Li, X.-F. (2018). Detection of continental-scale intensification of hourly rainfall extremes. *Nature Climate Change*, *8*(9), 803–807.

Haerter, J. O., & Berg, P. (2009). Unexpected rise in extreme precipitation caused by a shift in rain type? *Nature Geoscience*, *2*(6), 372–373.

Hardwick Jones, R., Westra, S., & Sharma, A. (2010). Observed relationships between extreme sub-daily precipitation, surface temperature, and relative humidity. *Geophysical Research Letters*, *37*(22).

Kottek, M., Grieser, J., Beck, C., Rudolf, B., & Rubel, F. (2006). World map of the Köppen-Geiger climate classification updated. *Meteorologische Zeitschrift*, *15*(3), 259–263.

Lenderink, G. *et al*. (2020) Scaling and responses of extreme hourly precipitation in three different climate change experiments with a convection-permitting model. Submitted to Phil. Trans. Roy. Soc. A.

Lenderink, G., Barbero, R., Loriaux, J. M., & Fowler, H. J. (2017). Super-Clausius–Clapeyron scaling of extreme hourly convective precipitation and its relation to large-scale atmospheric conditions. *Journal of Climate*, *30*(15), 6037–6052.

Lenderink, G., Mok, H. Y., Lee, T. C., & Van Oldenborgh, G. J. (2011). Scaling and trends of hourly precipitation extremes in two different climate zones-Hong Kong and the Netherlands. *Hydrology and Earth System Sciences*.

Lenderink, Geert, & Attema, J. (2015). A simple scaling approach to produce climate scenarios of local precipitation extremes for the Netherlands. *Environmental Research Letters*, *10*(8), 085001.

Lenderink, Geert, Barbero, R., Westra, S., & Fowler, H. J. (2018). Reply to comments on "Temperature-extreme precipitation scaling: A two-way causality?" *International Journal of Climatology*, *38*(12), 4664–4666.

Lenderink, Geert, & Van Meijgaard, E. (2008). Increase in hourly precipitation extremes beyond expectations from temperature changes. *Nature Geoscience*, *1*(8), 511–514.

Lenderink, Geert, & Van Meijgaard, E. (2010). Linking increases in hourly precipitation extremes to atmospheric temperature and moisture changes. *Environmental Research Letters*, *5*(2), 025208.

Lewis, E., Fowler, H., Alexander, L., Dunn, R., McClean, F., Barbero, R., Guerreiro, S., Li, X.-F., & Blenkinsop, S. (2019). GSDR: A global sub-daily rainfall dataset. *Journal of Climate*, *32*(15), 4715–4729.

Lewis, E., Quinn, N., Blenkinsop, S., Fowler, H. J., Freer, J., Tanguy, M., ... & Woods, R. (2018). A rule based quality control method for hourly rainfall data and a 1 km resolution gridded hourly rainfall dataset for Great Britain: CEH-GEAR1hr. *Journal of hydrology*, *564*, 930-943.

Li, X.-F., Blenkinsop, S., Barbero, R., Yu, J., Lewis, E., Lenderink, G., Guerreiro, S., Chan, S., Li, Y., & Ali, H. (2020). Global distribution of the intensity and frequency of hourly precipitation and their responses to ENSO. *Climate Dynamics*, *54*(11–12), 4823–4839.

Lochbihler, K., Lenderink, G., & Siebesma, A. P. (2017). The spatial extent of rainfall events and its relation to precipitation scaling. *Geophysical Research Letters*, *44*(16), 8629-8636.

Molnar, P., Fatichi, S., Gaál, L., Szolgay, J., & Burlando, P. (2015). Storm type effects on super Clausius–Clapeyron scaling of intense rainstorm properties with air temperature. *Hydrology and Earth System Sciences*, *19*(4), 1753.

Moron, V., Barbero, R., Evans, J. P., Westra, S., & Fowler, H. J. (2019). Weather Types and Hourly to Multiday Rainfall Characteristics in Tropical Australia. *Journal of Climate*, *32*(13), 3983-4011.

O'Gorman, P. A. (2015). Precipitation extremes under climate change. *Current Climate Change Reports*, *1*(2), 49–59.

Park, I.-H., & Min, S.-K. (2017). Role of convective precipitation in the relationship between subdaily extreme precipitation and temperature. *Journal of Climate*, *30*(23), 9527–9537.

Pfahl, S., O'Gorman, P. A., & Fischer, E. M. (2017). Understanding the regional pattern of projected future changes in extreme precipitation. *Nature Climate Change*, *7*(6), 423–427.

Pumo, D., Carlino, G., Blenkinsop, S., Arnone, E., Fowler, H., & Noto, L. V. (2019). Sensitivity of extreme rainfall to temperature in semi-arid Mediterranean regions. *Atmospheric Research*, *225*, 30–44.

Rajczak, J., & Schär, C. (2017). Projections of future precipitation extremes over Europe: A multimodel assessment of climate simulations. *Journal of Geophysical Research: Atmospheres*, *122*(20), 10–773.

Scherrer, S. C., Fischer, E. M., Posselt, R., Liniger, M. A., Croci-Maspoli, M., & Knutti, R. (2016). Emerging trends in heavy precipitation and hot temperature extremes in Switzerland. *Journal of Geophysical Research: Atmospheres*, *121*(6), 2626–2637.

Syafrina, A. H., Zalina, M. D., & Juneng, L. (2015). Historical trend of hourly extreme rainfall in Peninsular Malaysia. *Theoretical and Applied Climatology*, *120*(1–2), 259–285.

Trenberth, K. E., Dai, A., Rasmussen, R. M., & Parsons, D. B. (2003). The changing character of precipitation. *Bulletin of the American Meteorological Society*, *84*(9), 1205–1218.

Trenberth, K. E., & Shea, D. J. (2005). Relationships between precipitation and surface temperature. *Geophysical Research Letters*, *32*(14).

Utsumi, N., Seto, S., Kanae, S., Maeda, E. E., & Oki, T. (2011). Does higher surface temperature intensify extreme precipitation? *Geophysical Research Letters*, *38*(16).

Vittal, H., Ghosh, S., Karmakar, S., Pathak, A., & Murtugudde, R. (2016). Lack of dependence of Indian summer monsoon rainfall extremes on temperature: An observational evidence. *Scientific Reports*, *6*(1), 1–12.

Wasko, C., Parinussa, R. M., & Sharma, A. (2016). A quasi-global assessment of changes in remotely sensed rainfall extremes with temperature. *Geophysical Research Letters*, *43*(24), 12–659.

Wasko, Conrad, Sharma, A., & Johnson, F. (2015). Does storm duration modulate the extreme precipitation-temperature scaling relationship? *Geophysical Research Letters*, *42*(20), 8783–8790.

Westra, S., Fowler, H. J., Evans, J. P., Alexander, L. V., Berg, P., Johnson, F., Kendon, E. J., Lenderink, G., & Roberts, N. M. (2014). Future changes to the intensity and frequency of short-duration extreme rainfall. *Reviews of Geophysics*, *52*(3), 522–555.

Zhang, X., Zwiers, F. W., Li, G., Wan, H., & Cannon, A. J. (2017). Complexity in estimating past and future extreme short-duration rainfall. *Nature Geoscience*, *10*(4), 255–259.

Figure Captions

Fig. 1. Scaling rates (% K^{-1}) estimated using hourly precipitation (PPT) from the GSDR dataset (Lewis et al., 2019) and daily dewpoint temperature (DPT) from the HadISD dataset (Dunn et al. 2019). Scaling is estimated using the binning method at the 99^{th} percentile for 7088 gauges which have at least 12 years of hourly precipitation data. The number in blue indicates the number of gauges (NS) in each region and the number in black indicates the median scaling (% K^{-1}) for each region. The numbers below each panel indicate the percentage of gauges within each region which show scaling rates ranging from 0-0.5CC (green), 0.5CC-CC (orange), CC-1.5CC (brown), 1.5CC-2CC (pink), and greater than 2CC (red) respectively, where CC is 6.5%/K. This figure and subsequent figures were plotted using Generic Mapping Tool (GMT).

Fig. 2. Scaling rates (% K^{-1}) estimated using hourly precipitation (PPT) from the GSDR dataset (Lewis et al., 2019) and daily dewpoint temperature (DPT) from the HadISD dataset (Dunn et al. 2019). The scaling is estimated using the Zhang et al. [2017] method at the 99^{th} percentile for 7088 locations which have at least 12 years of daily precipitation data. The number in blue indicates the number of gauges (NS) in each region and the number in black indicates the median scaling (% K^{-1}) for each region. The numbers below each panel indicate the percentage of gauges within each region which show scaling

rates ranging from 0-0.5CC (green), 0.5CC-CC (orange), CC-1.5CC (brown), 1.5CC-2CC (pink), and greater than 2CC (red) respectively, where CC is 6.5%/K.

Fig. 3 (a) Latitudinal distribution of the 7088 hourly precipitation gauges (5-degree window size), (b) latitudinal variation of scaling, where red bars show median scaling for each 5-degree window and error bars show range of one standard deviation from the median scaling, (c) location of gauges that lie in wet (blue) and dry (red) regions based on annual maximum precipitation (R1xday) index (see Donat et al. 2016), (d) median scaling for wet and dry regions where error bars show one standard deviation from mean scaling, and (e-f) same as (c-d) but for wet and dry region classification based on total precipitation amount (PRCTOT) index. The dashed line shows the (6.5%/K) CC rate. The numbers in blue (red) indicate the number of stations lying in wet (dry) regions for the different classifications.

Fig. 4 (a, c, e, g). Scaling curves showing the dependency of extreme percentiles (95^{th}, cyan; 99^{th}, blue; 99.9^{th} pink) of the distribution of hourly precipitation on daily dewpoint temperature pooled for the C climate zone based on the Koppen-Geiger Climate classification. Note the logarithmic y-axis. Solid colour lines are percentiles computed for gauges at less than 400 m elevation, whereas dashed lines are for gauges at greater than 400m elevation. The horizontal lines at the bottom show interquartile ranges of DPT (1, 5, 25, 50, 75, 95, and 99%) for precipitation thresholds of 0.1mm (blue), 5mm (yellow), 20mm (red), and 50mm (pink) respectively). Dotted lines are the exponential relations given for 1 (black) and 2 (dark red) times CC scaling, and (b, d, f, g) probability distribution frequency (pdf) of scaling (99^{th} percentile) at individual gauges (solid lines for gauges at less than 400m elevation, and dotted lines for gauges at greater than 400m) within the specific region. The number at the top of the lower panels represents the median at-gauge scaling for the region. Statistical significance was estimated using KS tests for the distribution of the scaling.

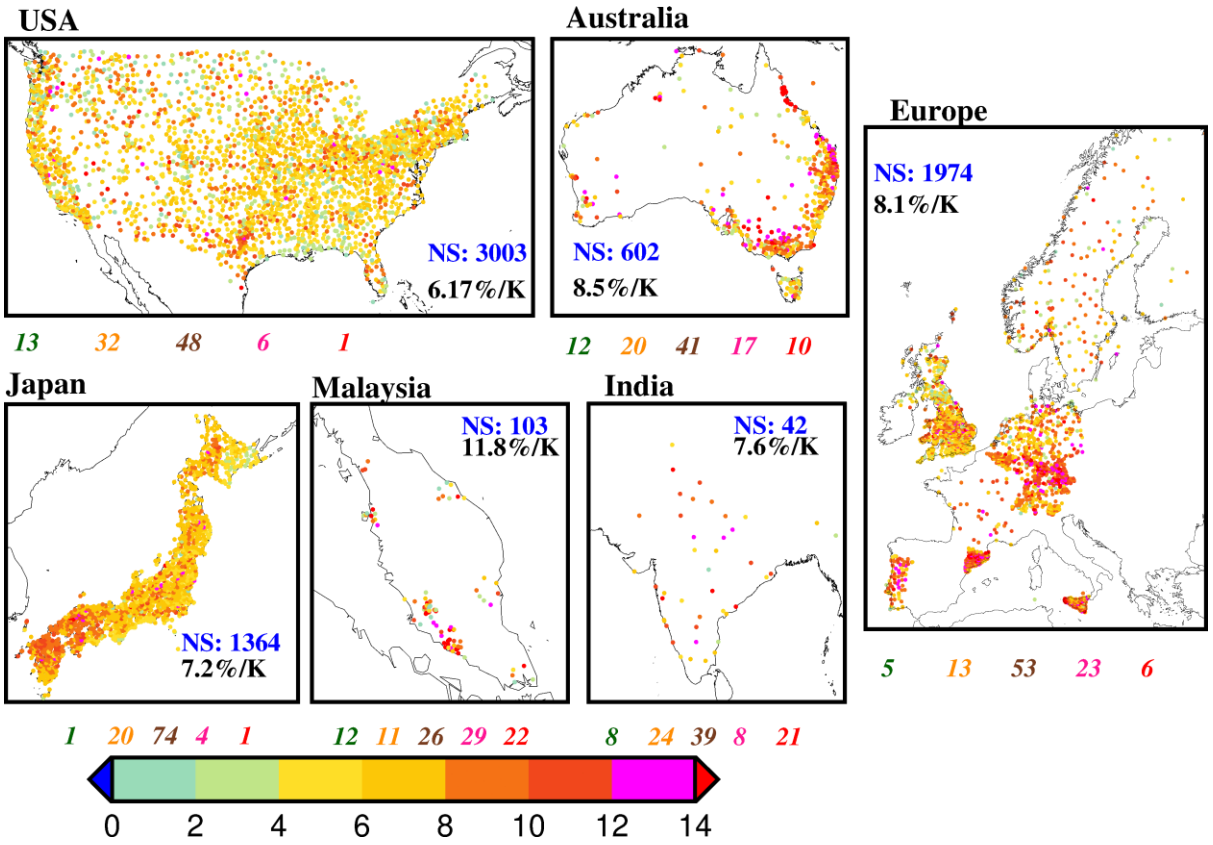

Fig. 1. Scaling rates (% K^{-1}) estimated using hourly precipitation (PPT) from the GSDR dataset (Lewis et al., 2019) and daily dewpoint temperature (DPT) from the HadISD dataset (Dunn et al. 2019). Scaling is estimated using the binning method at the 99th percentile for 7088 gauges which have at least 12 years of hourly precipitation data. The number in blue indicates the number of gauges (NS) in each region and the number in black indicates the median scaling (% K^{-1}) for each region. The numbers below each panel indicate the percentage of gauges within each region which show scaling rates ranging from 0-0.5CC (green), 0.5CC-CC (orange), CC-1.5CC (brown), 1.5CC-2CC (pink), and greater than 2CC (red) respectively, where CC is 6.5%/K. This figure and subsequent figures were plotted using Generic Mapping Tool (GMT).

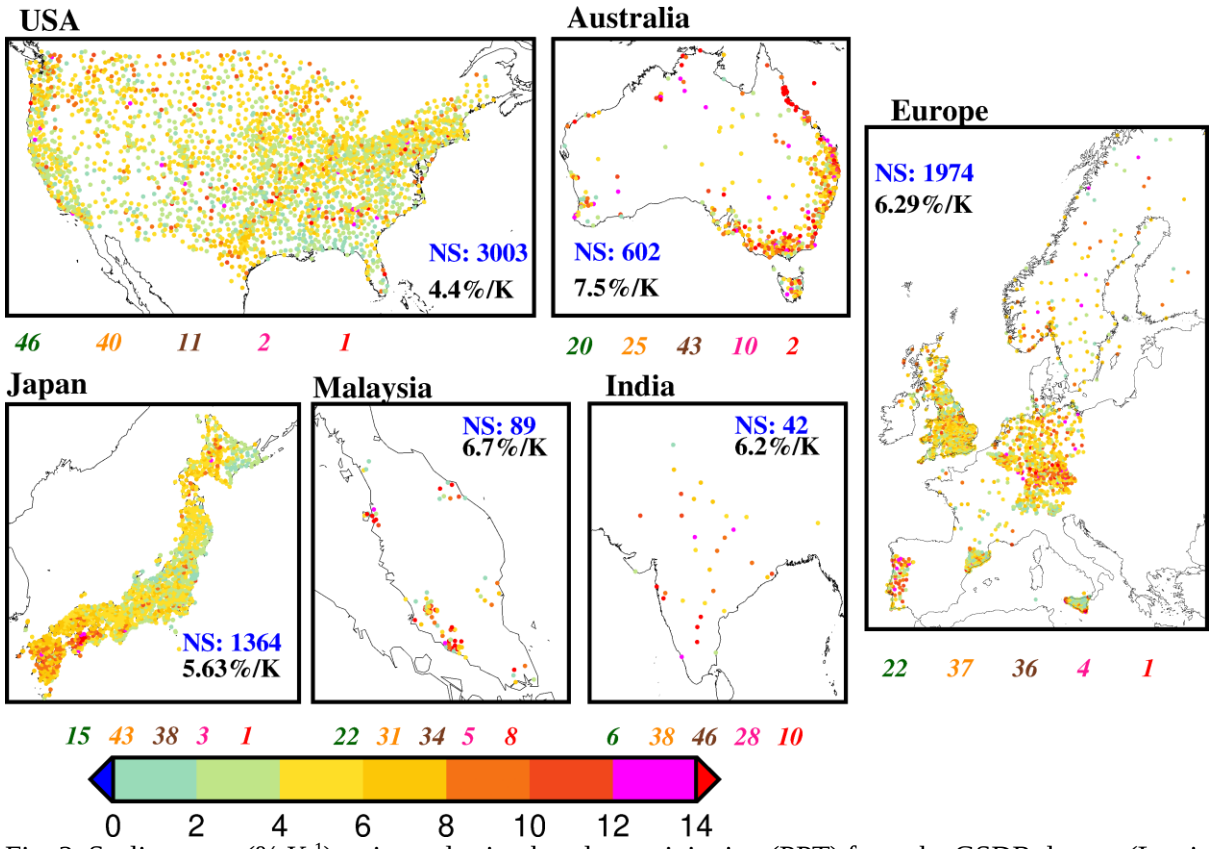

Fig. 2. Scaling rates (% K^{-1}) estimated using hourly precipitation (PPT) from the GSDR dataset (Lewis et al., 2019) and daily dewpoint temperature (DPT) from the HadISD dataset (Dunn et al. 2019). The scaling is estimated using the Zhang et al. [2017] method at the 99^{th} percentile for 7088 locations which have at least 12 years of daily precipitation data. The number in blue indicates the number of gauges (NS) in each region and the number in black indicates the median scaling (% K^{-1}) for each region. The numbers below each panel indicate the percentage of gauges within each region which show scaling rates ranging from 0-0.5CC (green), 0.5CC-CC (orange), CC-1.5CC (brown), 1.5CC-2CC (pink), and greater than 2CC (red) respectively, where CC is 6.5%/K.

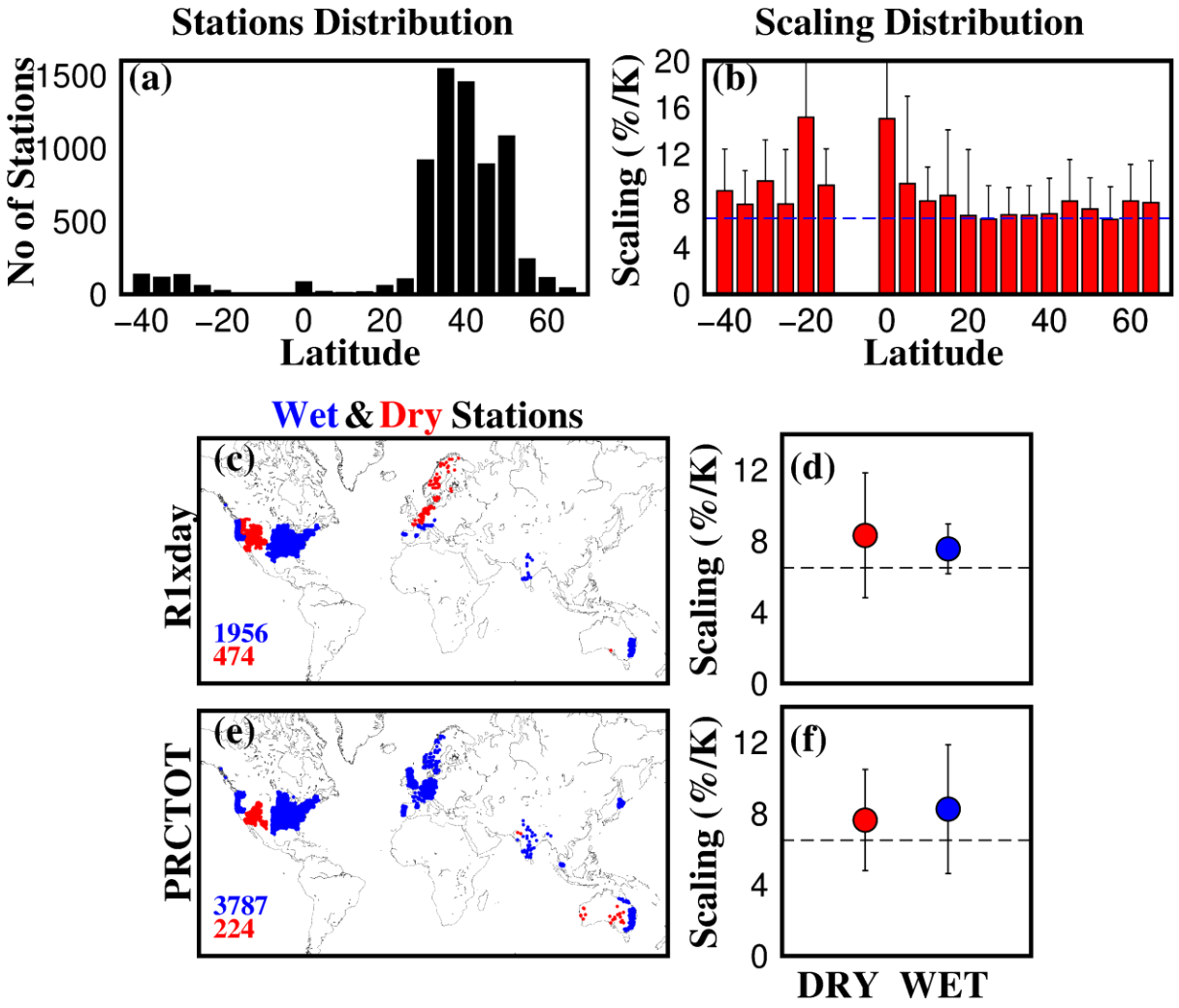

Fig. 3 (a) Latitudinal distribution of the 7088 hourly precipitation gauges (5-degree window size), (b) latitudinal variation of scaling, where red bars show median scaling for each 5-degree window and error bars show range of one standard deviation from the median scaling, (c) location of gauges that lie in wet (blue) and dry (red) regions based on annual maximum precipitation (R1xday) index (see Donat et al. 2016), (d) median scaling for wet and dry regions where error bars show one standard deviation from mean scaling, and (e-f) same as (c-d) but for wet and dry region classification based on total precipitation amount (PRCTOT) index. The dashed line shows the (6.5%/K) CC rate. The numbers in blue (red) indicate the number of stations lying in wet (dry) regions for the different classifications.

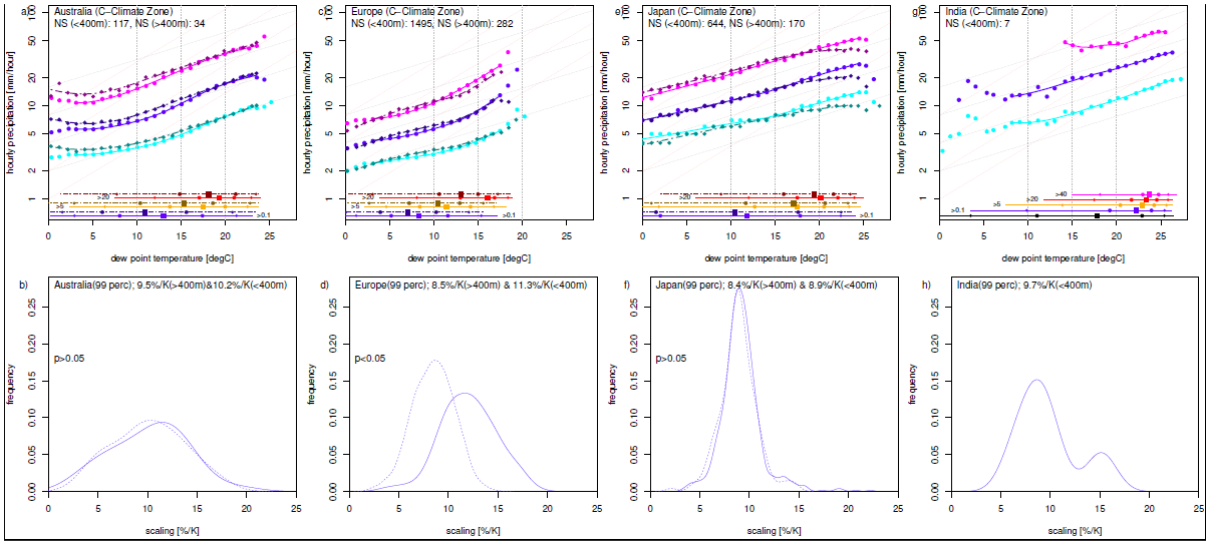

Fig. 4 (a, c, e, g). Scaling curves showing the dependency of extreme percentiles (95th, cyan; 99th, blue; 99.9th pink) of the distribution of hourly precipitation on daily dewpoint temperature pooled for the C climate zone based on the Koppen-Geiger Climate classification. Note the logarithmic y-axis. Solid colour lines are percentiles computed for gauges at less than 400 m elevation, whereas dashed lines are for gauges at greater than 400m elevation. The horizontal lines at the bottom show interquartile ranges of DPT (1, 5, 25, 50, 75, 95, and 99%) for precipitation thresholds of 0.1mm (blue), 5mm (yellow), 20mm (red), and 50mm (pink) respectively). Dotted lines are the exponential relations given for 1 (black) and 2 (dark red) times CC scaling, and (b, d, f, g) probability distribution frequency (pdf) of scaling (99th percentile) at individual gauges (solid lines for gauges at less than 400m elevation, and dotted lines for gauges at greater than 400m) within the specific region. The number at the top of the lower panels represents the median at-gauge scaling for the region. Statistical significance was estimated using KS tests for the distribution of the scaling.

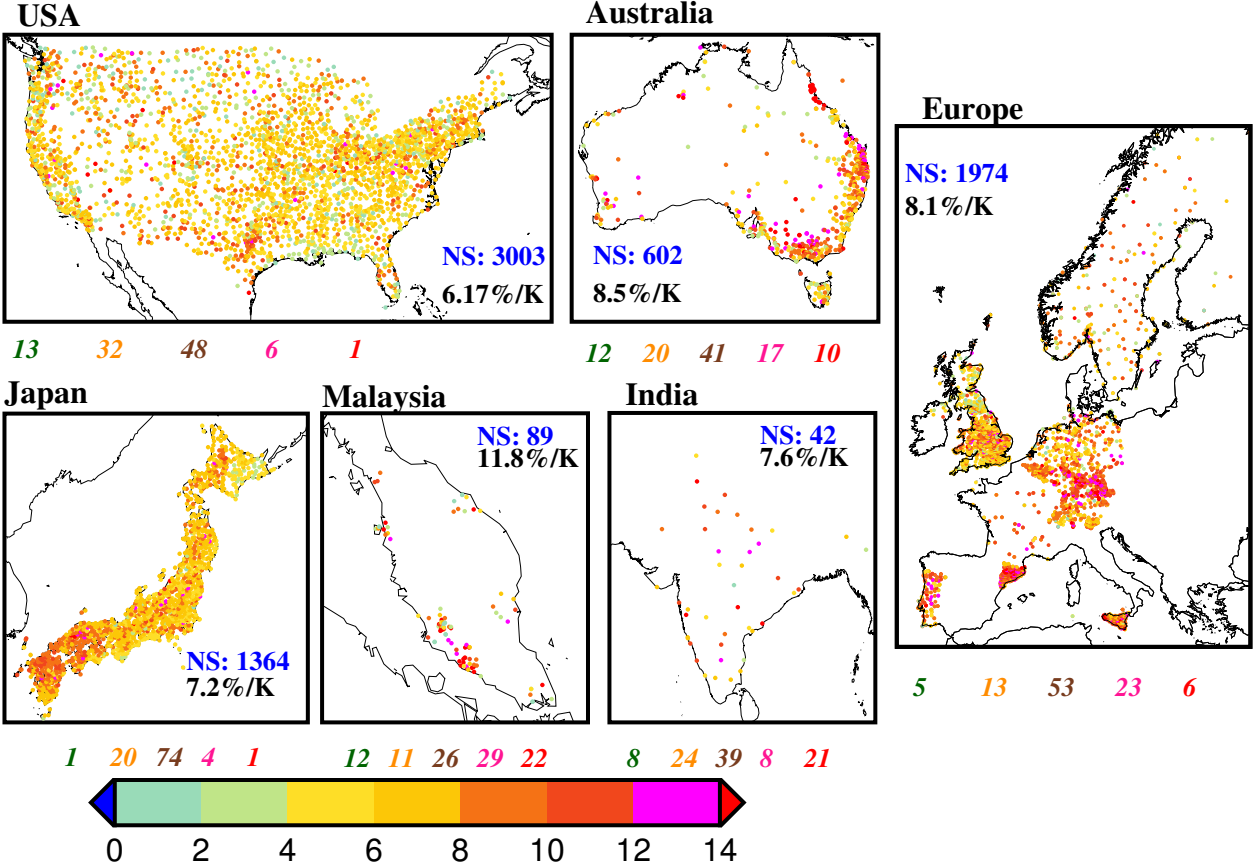
USA
NS: 3003
6.17%/K
13 32 48 6 1
Australia
NS: 602
8.5%/K
12 20 41 17 10
Europe
NS: 1974
8.1%/K
5 13 53 23 6
Japan
NS: 1364
7.2%/K
1 20 74 4 1
Malaysia
NS: 89
11.8%/K
12 11 26 29 22
India
NS: 42
7.6%/K
8 24 39 8 21
0 2 4 6 8 10 12 14

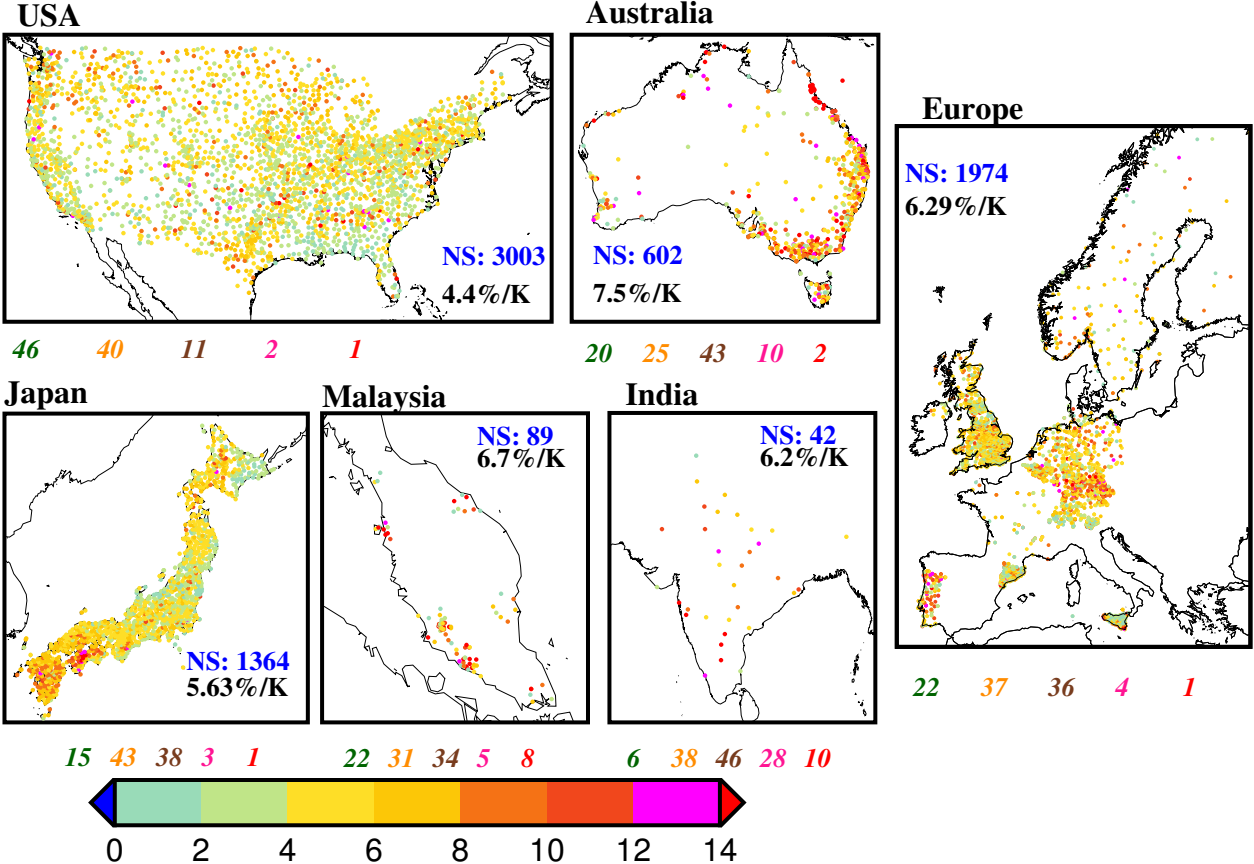
USA
NS: 3003
4.4%/K
46 40 11 2 1
Australia
NS: 602
7.5%/K
20 25 43 10 2
Europe
NS: 1974
6.29%/K
22 37 36 4 1
Japan
NS: 1364
5.63%/K
15 43 38 3 1
Malaysia
NS: 89
6.7%/K
22 31 34 5 8
India
NS: 42
6.2%/K
6 38 46 28 10
0 2 4 6 8 10 12 14

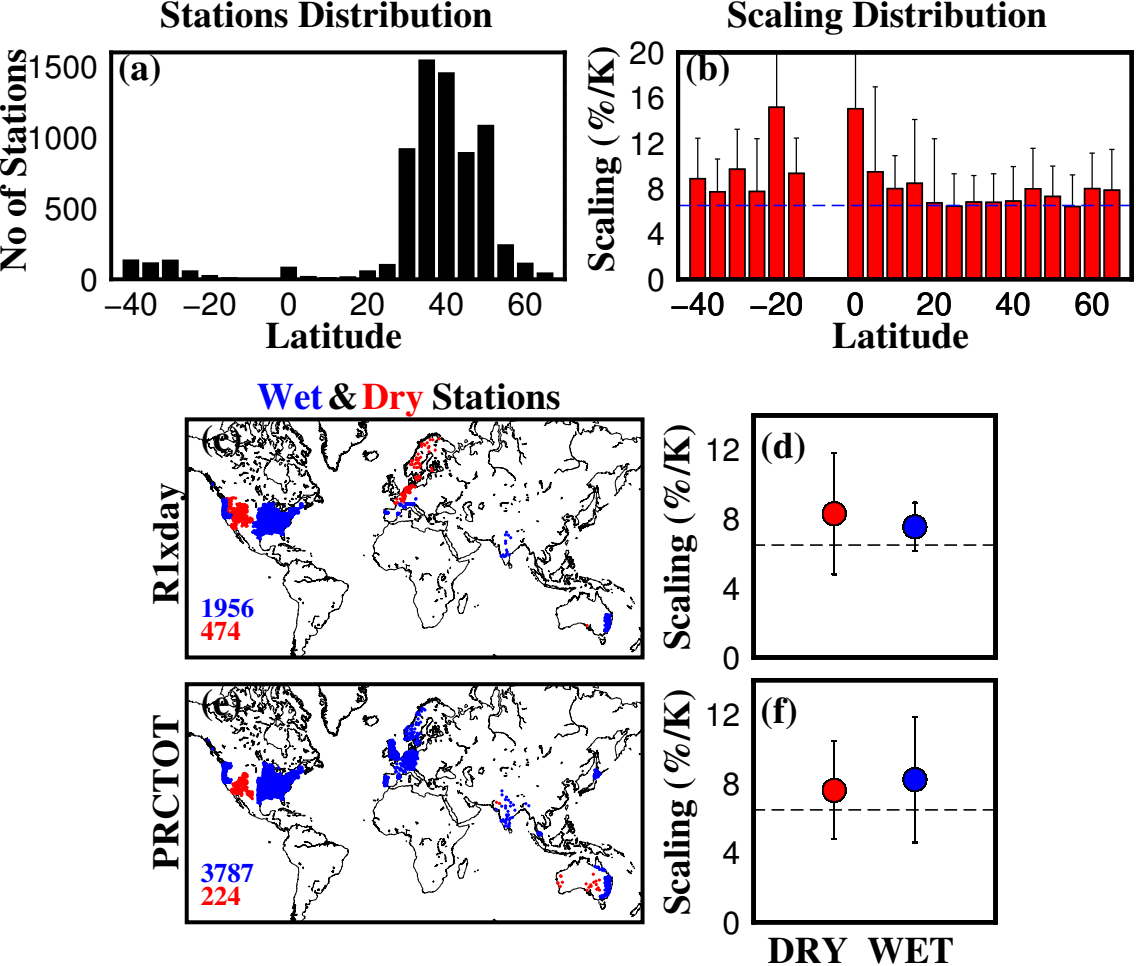
Stations Distribution
(a)
No of Stations
1500
1000
500
0
−40
−20
0
20
40
60
Latitude
Scaling Distribution
(b)
Scaling (%/K)
20
16
12
8
4
0
−40
−20
0
20
40
60
Latitude
Wet & Dry Stations
R1xday
1956
474
(d)
Scaling (%/K)
12
8
4
0
PRCTOT
3787
224
(f)
Scaling (%/K)
12
8
4
0
DRY
WET

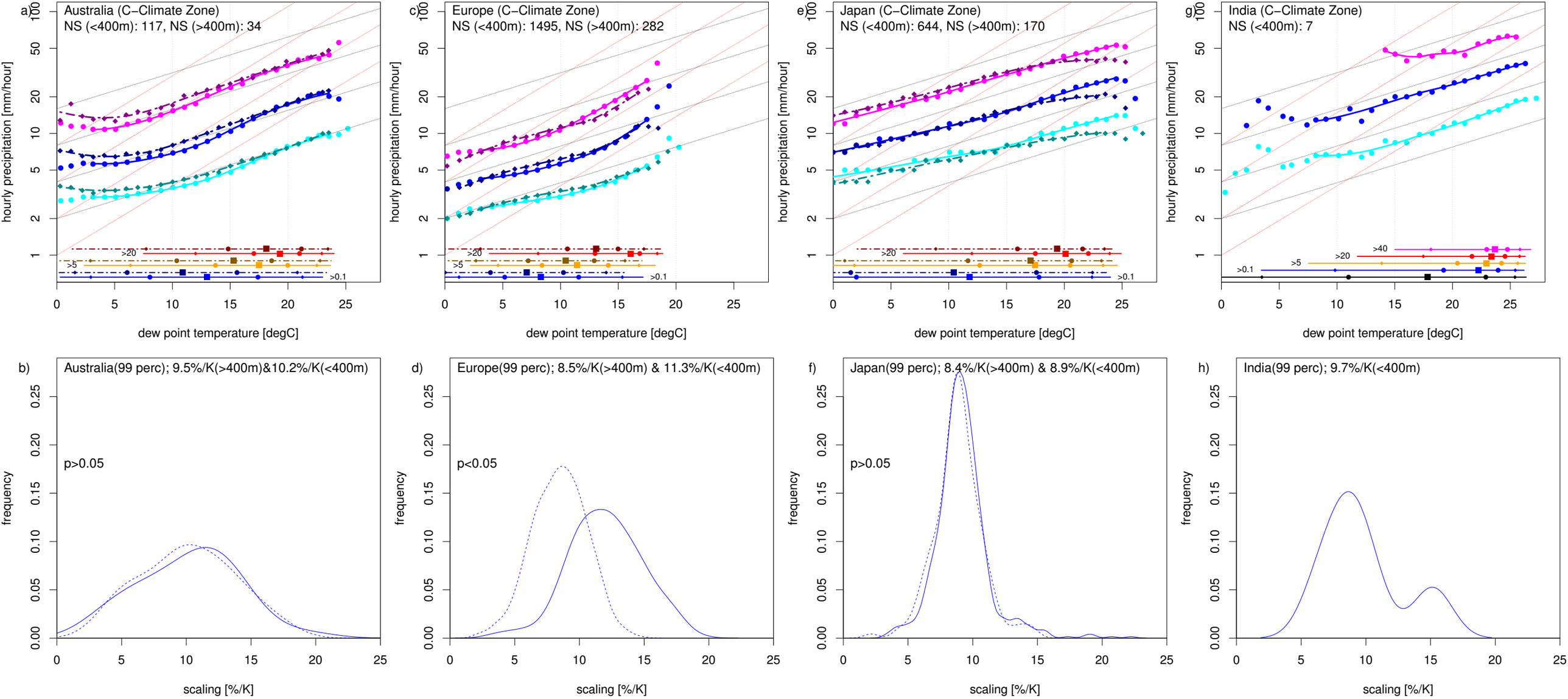
a)
Australia (C−Climate Zone)
NS (<400m): 117, NS (>400m): 34
hourly precipitation [mm/hour]
dew point temperature [degC]
>20
>5
>0.1
b)
Australia(99 perc); 9.5%/K(>400m)&10.2%/K(<400m)
p>0.05
frequency
scaling [%/K]
c)
Europe (C−Climate Zone)
NS (<400m): 1495, NS (>400m): 282
d)
Europe(99 perc); 8.5%/K(>400m) & 11.3%/K(<400m)
p<0.05
e)
Japan (C−Climate Zone)
NS (<400m): 644, NS (>400m): 170
f)
Japan(99 perc); 8.4%/K(>400m) & 8.9%/K(<400m)
p>0.05
g)
India (C−Climate Zone)
NS (<400m): 7
>40
h)
India(99 perc); 9.7%/K(<400m)